Oblique MHD Cosmic-Ray Modified Shocks: Two-Fluid Numerical Simulations

Adam Frank[1], T. W. Jones[1] and Dongsu Ryu[2,3]

[1]Department. of Astronomy, University of Minnesota, Minneapolis, MN 55455
[2]Princeton University Observatory, Peyton Hall, Princeton, NJ 08544
[3]Department of Astronomy & Space Science, Chungnam National University, Daejeon 305-764, Korea

Abstract

We present the first results of time dependent two-fluid cosmic-ray (CR) modified MHD shock simulations. The calculations were carried out with a new numerical code for 1-D ideal MHD. By coupling this code with the CR energy transport equation we can simulate the time-dependent evolution of MHD shocks including the acceleration of the CR and their feedback on the shock structures. We report tests of the combined numerical method including comparisons with analytical steady state results published earlier by Webb, as well as internal consistency checks for more general MHD CR shock structures after they appear to have converged to dynamical steady states. We also present results from an initial time dependent simulation which extends the parameter space domain of previous analytical models. These new results support Webb's suggestion that equilibrium oblique shocks are less effective than parallel shocks in the acceleration of CR. However, for realistic models of anisotropic CR diffusion, oblique shocks may achieve dynamical equilibrium on shorter timescales than parallel shocks.

1. Introduction

Nonlinear theories of diffusive shock acceleration have demonstrated the importance of cosmic-ray (CR) feedback on the evolution of shock structures (e.g., Blandford & Eichler 1987). Using two-fluid models it has been shown (e.g. Drury& Völk 1981, Achterberg *et. al.* 1984, Kang & Jones 1990) that CR pressures can become large enough to smooth shocks, eliminating the entropy generating gas sub-shock. More generally, the CR feedback modifies the efficiency of energy transfer from gas to CR in the shock. Recent numerical simulations (e.g., Drury & Falle 1987, Falle & Giddings 1989, Jones & Kang 1990, Kang & Jones 1991, Kang, Jones & Ryu 1992) have also shown the importance of time-dependent effects in the determination of CR modified shock properties. For the most part, past studies of CR modified shocks have focused on pure hydrodynamical, (or parallel, sonic mode) models of the shock dynamics. Magnetic fields, however, will generally be dynamically important in many environments where particle acceleration occurs. It has been suggested that components of the magnetic field which are aligned perpendicular to the shock normal (tangent to the shock face) can alter the efficiency of the acceleration process. Jokipii (1987) has pointed out that, for standard models of CR anisotropic diffusion (see equation [4.1] below) perpendicular components of the field will decrease the shock crossing time for a CR particle, increasing the rate at which individual particles gain energy from the shock. On the other hand, Baring, Ellison & Jones (1993) have shown that the efficiency of thermal particle injection into the CR population can be dramatically decreased by perpendicular magnetic field components. ¿From these examples it is clear that to understand the fundamental nature of shock acceleration in more realistic astrophysical settings, full MHD calculations are needed. Two-fluid models of CR transport along the lines introduced by Drury & Völk (1981) are an efficient means to begin such explorations. Such models enable one to economically calculate the dynamical features of flows within the constraints imposed by the need to estimate *a priori* some closure parameters for the CR. Equilibrium MHD CR-modified shock structures have been calculated by Webb (1983) using these methods for the case where the gas is cold and its pressure can be ignored. Webb's calculations demonstrated that, as for the CR-modified gas dynamic flows, both sub-shock and smoothed, CR dominated solutions to the MHD CR shock equations were possible. However, his solutions suggested that, in the limited range of conditions he could consider, shock acceleration of cosmic-rays was less effective when the upstream tangential components of the field were strong. Among other consequences this appears to expand the portions of the shock parameter space that lead to sub-shock solutions. That could impact on such issues as low energy injection processes and the momentum distribution of the CR.

Some subsequent steady state two-fluid analyses, considering a wider parameter space support the above impressions (Kennel *et al* 1985, Webb *et al* 1986). In this paper we report the first results of time dependent MHD CR two-fluid simulations. We present tests of a new numerical code against Webb's analytical models as well as more general internal checks on the code's ability to evolve shocks to self-consistent steady state MHD CR structures. Our simulations confirm Webb's calculations. Our numerical models also allow

us to extend Webb's calculations by lifting the cold gas, ($P_g = 0$), restriction to examine the effects of a full range of initial parameters on CR-modified MHD shock structures.

2. Methods

We solve the equations of ideal MHD for one dimensional flow in Cartesian coordinates (e.g., Jeffrey 1968). As with two-fluid gas dynamic models the conservation equations are modified to include momentum and energy source terms from CR feedback (e.g., Drury & Völk, 1981, Jones & Kang, 1990). The MHD equations are written in conservative, vector form as

$$\frac{\partial \mathbf{q}}{\partial t} + \frac{\partial \mathbf{F}}{\partial x} = \mathbf{S}. \tag{2.1}$$

with

$$\mathbf{q} = \begin{pmatrix} \rho \\ \rho u_x \\ \rho u_y \\ \rho u_z \\ B_y \\ B_z \\ E \end{pmatrix}, \tag{2.2}$$

and

$$\mathbf{F} = \begin{pmatrix} \rho u_x \\ \rho u_x^2 + P^* - B_x^2 \\ \rho u_x u_y - B_x B_y \\ \rho u_x u_z - B_x B_z \\ B_y u_x - B_x u_y \\ B_z u_x - B_x u_z \\ (E + p^*) u_x - B_x (B_x u_x + B_y u_y + B_z u_z) \end{pmatrix}, \tag{2.3}$$

while the CR source term vector is

$$\mathbf{S} = - \begin{pmatrix} 0 \\ \partial P_c / \partial x \\ 0 \\ 0 \\ 0 \\ 0 \\ u_x \partial P_c / \partial x + S_e \end{pmatrix}. \tag{2.4}$$

The CR are themselves treated as a massless, diffusive fluid through a conservation equation for the CR energy, E_c, derived from the diffusion-advection equation (Skilling 1975); namely,

$$\frac{\partial E_c}{\partial t} + \frac{\partial u_x E_c}{\partial x} = \frac{\partial}{\partial x} \left(\kappa \frac{\partial E_c}{\partial x} \right) - P_c \frac{\partial u_x}{\partial x} + S_e. \tag{2.4}$$

In these relations

$$P^* = P_g + \frac{1}{2}(B_x^2 + B_y^2 + B_z^2), \tag{2.5}$$

$$E = \frac{1}{2}\rho(u_x^2 + u_y^2 + u_z^2) + \frac{1}{(\gamma_g - 1)} P + \frac{1}{2}(B_x^2 + B_y^2 + B_z^2), \tag{2.6}$$

$$P_c = (\gamma_c - 1)E_c. \tag{2.7}$$

and the magnetic field components are expressed in rationalized units

$$B \rightarrow \frac{B}{\sqrt{4\pi}}. \tag{2.8}$$

In the expressions presented above the following definitions hold: ρ is the mass density; u_x, B_x and u_y, u_z, B_y, B_z are the components of velocity and magnetic field parallel and perpendicular to shock front; P_g, γ_g and P_c, γ_c are the gas and cosmic-ray pressures and adiabatic indices, and κ is the energy weighted spatial diffusion coefficient for the CR parallel to the shock normal. The quantity S_ϵ is a term that allows direct energy transfer from the gas to the CR, such as through the low energy injection of thermal particles into the CR population (e.g., Jones & Kang 1990). This is introduced for completeness, but for the present, we set $S_\epsilon = 0$. In this discussion we set $\gamma_g = 5/3$, while γ_c, which depends upon the mix of nonrelativistic and relativistic particles in the CR population, will be treated as an input parameter. In general both γ_c and κ are properties of the solution, so the need to specify their properties *a priori* is the major drawback of the two-fluid model.

In the interest of simplicity we will not consider here flows with tangential magnetic field rotations, although the numerical code is quite capable of handling such features. Thus, without further loss of generality we can place the magnetic field in the X-Z plane, $\vec{B} = (B_x, 0, B_z)$. We will also restrict ourselves to flows with no upstream tangential velocity, $u_y = u_z = 0$. All of the simulations discussed here are essentially piston driven shock tubes. We establish the flows by projecting magnetized fluid with embedded CR in from the right boundary, using an open boundary condition and reflecting it off a wall (piston) at the left boundary. The tangential magnetic field at the left boundary is "mirrored" in the same manner as the gas density. Previous simulations of CR modified shocks have shown that their time to evolve to dynamical equilibrium scales with the so-called diffusion time, t_d, (e.g. Jones & Kang 1990), which in the present case is conveniently expressed as

$$t_d = \frac{\kappa}{u_s^2}, \tag{2.9}$$

where u_s is the shock speed (see equation. 3.2). In our discussion below we will express simulation times in units of t_d, appropriate to that simulation. The width of a CR-modified shock transition scales with the related diffusion length scale, x_d,

$$x_d = \frac{\kappa}{u_s} = t_d u_s. \tag{2.10}$$

To obtain accurate numerical results with the methods we employ it is important that computation zones be small enough to resolve the diffusive shock features on this scale. For our discussion we define, therefore, the resolution ratio of each simulation to be,

$$n_r = \frac{x_d}{\Delta x}. \tag{2.11}$$

Our numerical method solves equation [2.1] through the second order finite difference "Total Variation Diminishing" (TVD) gas dynamics method of Harten (Harten 1981)

extended to MHD (Ryu & Jones 1993). The pure MHD (**S** = 0) form of the equation is solve with the aid of an approximate Riemann solver, used to estimate the fluxes, **F**. CR source corrections, **S**, are then added in a manner preserving second order accuracy. Shocks and other discontinuities are generally resolved within a few zones. The CR energy equation is solved using a second order combined monotone advection and Crank-Nicholson scheme. Further details of the method will be presented elsewhere (Frank, Jones & Ryu, in preparation). A pure gas dynamical version of the code was tested against both analytical steady state solutions and numerical time dependent models calculated with our well-tested PPM code (Jones & Kang 1990), with excellent agreement. The pure MHD code was tested against a variety of 1-D shock tube problems involving all three families of MHD waves using a nonlinear MHD Riemann solver (Ryu & Jones 1993).

3. Results: Comparisons with Analytical Models

In order to test the accuracy of our numerical method we first attempted to reproduce the analytical steady state solutions of Webb (1983). In that paper Webb demonstrated in addition to discontinuous gas "sub-shock" solutions with a smooth CR shock precursor, that one may obtain completely smooth "shock" solutions to the MHD CR equations if the downstream velocity remains super-Alfvénic and the upstream CR pressure, P_c, is high. That behavior is analogous to smooth gas dynamic shock solutions identified earlier by Drury & Völk (1981). However, Webb was able to consider only flows in which the upstream gas was cold; i.e., in which $P_g = 0$.

In figures 1 and 2 we present the time-asymptotic shock structures formed in numerical simulations with upstream conditions corresponding to those in Webb's paper (his figure 7 and figure 8). The upstream conditions for these simulations are given, as models 1 and 2, in table 1. These simulations were performed with a constant CR diffusion coefficient, $\kappa = .01$. The resolution ratios, n_r, for models 1 and 2 are $n_r = 21$ and 32 respectively. The Alfvénic Mach numbers for models 1 and 2 are $M_a = u_p\sqrt{\rho}/B_x = 1$ and 2 respectively where u_p is the piston speed. In these models $\gamma_c = 4/3$. The simulations where carried out until the postshock state appeared steady; namely, $t \sim 30t_d$. The resultant shock transformations provide excellent agreement with our best estimates of the downstream states found by Webb. The largest uncertainties in the comparison are, in fact, the determination of the downstream states from Webb's figures. For model 2 the entropy, $s = log(P_g/\rho^{\gamma_g})$, (not shown in the figure) increases though the shock, demonstrating that the flow contains an MHD fast mode sub-shock, as predicted by Webb. The entropy for the flow in figure 1 shows no increase, again as predicted. Recall that these particular calculations were meant to be carried out under Webb's cold gas ($P_g \approx 0$) restriction. For numerical reasons the upstream gas pressure was set in practice to be a small fraction (10^{-3}) of the CR pressure. As an additional comparison we have also reproduced the pure perpendicular ($B_x = 0$) smooth and MHD sub-shock models of Webb with the accuracy comparable to that shown in figures 1 and 2.

Our previous simulations of CR-modified gas shocks required numerical grids that over resolved the CR shock precursor by roughly a factor of 10 to assure high accuracy (Jones &

Kang 1990). In order to explore the dependence of the accuracy on numerical resolution for these MHD simulations we have run a series of tests with the upstream conditions of model 2, varying the numerical resolution. We ran simulations with $n_r = 4, 8, 16, 32$. In figure 3 we plot a measure of the fractional error in the downstream CR pressure, (compared with the value for the highest resolution case, $n_r = 32$),

$$\frac{\epsilon_c = P_c(n_r) - P_c(32)}{P_c(32).} \tag{3.1}$$

The Figure shows that the simulated shocks converge quickly once $n_r > 10$. As mentioned above, that state is in good agreement with Webb's analytical result. The converged numerical postshock CR pressure that is about 4% higher than our estimate of Webb's result, although we attribute much of this error to uncertainties in reading final states from published figures rather than tables. These results agree well with previously mentioned gas dynamic behaviors found by Jones & Kang (1990). We believe the limiting factor to be the accuracy of the Crank-Nicholson method used for updating the diffusive CR energy equation. As a further test of the numerical method we have performed tests of the self-consistency of more general steady state MHD CR shock solutions. This was done by testing the accuracy of various MHD jump conditions for apparently steady shocks in the shock frame. For example, the various momentum components of the full flux vector, **F**, in equation [2.3] should be the same across the shock when measured in that frame (with F_2 corrected to include P_c). The shock velocity for this exercise was determined from the conservation of mass equation for a steady shock transformed into the piston frame; namely,

$$u_s = \frac{[\rho u]}{[\rho]}. \tag{3.2}$$

where [ ] refers to differences across the shock. We find that for the simulations with $n_r > 10$ the jump conditions were satisfied to better than one part in 1×10^4.

4. Finite Gas Temperature MHD Shocks

Since our numerical code solves the full MHD CR two-fluid equations there is no need to restrict investigations to those cases where $P_g = 0$. In figure 4 we present the results from a simulation of an MHD CR shock formed from gas of finite upstream pressure, P_g. The upstream conditions for this simulation, model 4, is presented in table 1. We note that the sonic Mach number in this case is $M_s = 4$. The Alfvénic Mach number $M_a = 12$. Standard weak scattering models of particle diffusion lead to differences in diffusion across and along field lines. Thus κ, which controls diffusion along the shock normal should depend on the angle between field and the shock normal, $\phi = tan^{-1}(\frac{B_z}{B_x})$. Thus we adopt κ of a form, (e.g., Webb 1983, Jokipii 1987, Zank *et. al.* 1990),

$$\kappa = \kappa_{||} \cos^2 \phi + \kappa_{\perp} \sin^2 \phi, \tag{4.1}$$

where the directions $||$ and $\perp$ refer to the magnetic field direction. Note, of course, that ϕ is generally a changing function of space and time. For this initial exploration we arbitrarily set $\kappa_{||} = .01 = 10 \times \kappa_{\perp}$.

In general P_c develops more rapidly for a stiffer CR equation of state (Jones & Kang 1990). Thus, in order to keep the computational costs low for these first tests we used $\gamma_c = 5/3$ in the following model. This would influence the detailed properties of the steady state flow, but will not alter the qualitative character in ways that are important to the present discussion.

In figure 4 we illustrate the evolution of a time dependent, finite gas pressure simulation. In this model the upstream magnetic field angle is $\varphi_o = 30^o$. We present results at three different times: $t = 12, 24$, and $36 t_d$. Since κ is not a constant in space or time in this simulation, we define t_d here in terms of $\kappa = 0.01$. Figure 4 shows a strong fast mode shock driven by the piston. That shock has become almost smoothed by the CR pressure. Comparisons of this model with an analogous parallel field ($\varphi = 0^o$) simulations show a number important differences. First, the parallel shock model reaches a dynamical steady state more slowly than the oblique shock case. That is simply because, according to equation [4.1] the diffusion coefficient, κ, in the parallel case is greater, so that energy gain by the CR is slowed (e.g., Jokipii 1987). On the other hand, while the dynamical steady state may be reached more quickly in oblique shocks than in parallel shocks the effectiveness of the acceleration in the oblique case is reduced. The downstream value of P_c in the oblique shock case is decreased by 8% from what is obtained in the parallel shock model. It is reasonable to expect that in the oblique models the upstream momentum flux which would have gone into accelerating CR is being used to do work on the tangential magnetic field. We note that behind the fast mode shock a weaker slow mode shock compresses the CR driven transition density spike (see Jones & Kang 1990 for a discussion of this feature). Close examination also shows that CR particle acceleration is taking place as that slow mode shock develops. Modification of the density spike, which can only be seen in time dependent models, is an example the additional complications which arise due to the multiple wave families present in MHD.

5. Conclusions

1) The numerical code we have developed accurately computes two-fluid models of CR-modified MHD shocks. If the resolution ratio defined in the text, $n_r > 10$, then the time asymptotic properties of the simulations appear to converge to analytically predicted steady states. The time asymptotic numerical shocks are also internally consistent in terms of conservation laws expected to be satisfied across steady shocks to at least one part in 10^4.

2) Because of the work done on tangential fields within the shocks, time asymptotic particle acceleration will tend to be more efficient in parallel shocks than in oblique shocks. However, the oblique shocks reach dynamical steady states more quickly for a given diffusion coefficient parallel to the magnetic field.

3) Transient features develop from the MHD fast mode CR shocks similar to those seen in pure CR hydrodynamical shocks. However, these transients are modified and made more complex by the development of MHD slow mode shocks.

Acknowledgments

This work was supported in part by NASA through grant NAGW-2548, the NSF through grant AST-9100486 and by the University of Minnesota Supercomputer Institute.

References

Achterberg, A., Blandford, R.D. & Periwal, V. 1984, A&A, 98, 195.

Baring, M. G., Ellison, D. C., & Jones, F. C. 1993, ApJ, in press.

Blandford, R.D. & Eichler, D. 1987, Phys Rept, 154, 1.

Drury, L. O'C., & Völk, H. J. 1981, ApJ, 248, 344.

Drury, L. O'C., & Falle, S. A. E. G. 1986, MNRAS, 223, 353.

Falle, S. A. E. G., & Giddings J. R. 1987, MNRAS, 225, 399.

Harten, A. 1983, J. Comp. Phys., 49, 357.

Jeffrey, A. 1966, *Magnetohydrodynamics* (London: Oliver and Boyd).

Jokipii, J. R. 1987, ApJ, 313, 846.

Jones, T. W. & Kang, H. 1990, ApJ, 363, 499.

Kang, H., & Jones, T. W. 1990, ApJ, 353, 149.

Kang, H., & Jones, T. W. 1991, MNRAS, 249, 439.

Kang, H., Jones, T. W., & Ryu, D. 1992, ApJ, 385, 193.

Kennel, C. F., Edmiston, J. P. & Hada, T. 1985, in *Collisionless Shocks in the Heliosphere: A Tutorial Review*, ed. Robert G. Stone & Bruce Tsurutani (American Geophysical Union: Washington, D. C.), p.1.

Ryu, D., & Jones, T. W. 1993, ApJ, to be submitted.

Skilling, J. 1975, MNRAS, 172, 557.

Webb, G. M. 1983, A&A, 127, 97.

Webb, G. M., Drury, L. O'C. & Völk H. J. 1986, A&A, 160, 335.

Zank, G.P., Axford, W. I., & McKenzie, J. F. 1990, A&A, 233, 275.

Figure Captions

Fig. 1.— Model 1 in table 1. MHD CR shock transition region for a piston driven shock with upstream conditions taken from figure 7 of Webb (1983). Shown are the density, ρ, normal component of velocity, u_x, tangential velocity, u_z, tangential component of magnetic field, B_z, magnetic field orientation angle, $\phi = tan^{-1}(\frac{B_z}{B_x})$, and cosmic-ray pressure, P_c. See table 1 for upstream flow conditions. The abscissa is given in units of diffusion length $x_d = \kappa/u_s$. The dashed lines are post-shock values taken from Webb's figure 7, except in the plot of u_z where the value was calculated using equation [3.2] and the MHD steady state jump conditions.

Fig. 2.– Model 2 from table 1. MHD CR Shock transition region for a piston driven shock with upstream conditions taken from Webb's figure 8.

Fig. 3.– Fractional error (equation [3.1] in the computed value of the post-shock CR pressure, P_c, in model 1 as a function of resolution, $n_r = x_d/\Delta x$.

Fig. 4.– Model 3 from table 1. This model has an upstream field orientation, $\phi_o = 30^o$. Results are shown at $t = 12, 24$ and $36 t_d$.

Table 1
Upstream Conditions for Models

Model	ρ	U_p	B_x	B_z	P_g	P_c	κ	Transition
1	1	.2	.32	.45	0.0	.25	.01	smooth
2	1	.2	.32	.32	0.0	.075	.01	sub-shock
3	1	.2	.05	.03	1.49×10^{-3}	1.49×10^{-3}	$\kappa(\mathbf{B})$	smooth

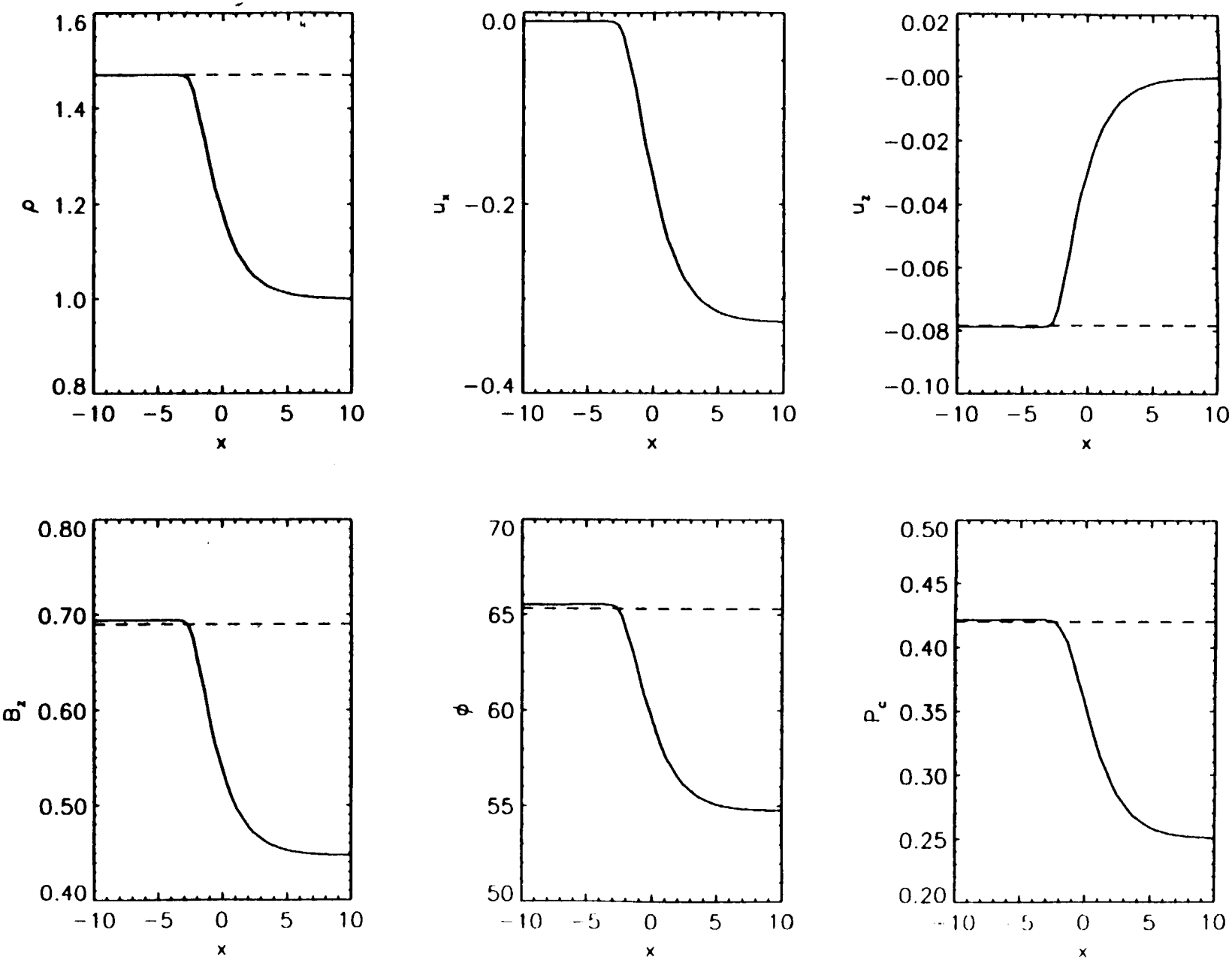
1.6
1.4
1.2
1.0
0.8
ρ
−10 −5 0 5 10
x
0.0
−0.2
−0.4
u_x
−10 −5 0 5 10
x
0.02
−0.00
−0.02
−0.04
−0.06
−0.08
−0.10
u_z
−10 −5 0 5 10
x
0.80
0.70
0.60
0.50
0.40
B_z
−10 −5 0 5 10
x
70
65
60
55
50
Φ
−10 −5 0 5 10
x
0.50
0.45
0.40
0.35
0.30
0.25
0.20
P_e
−10 −5 0 5 10
x

Fig. 1

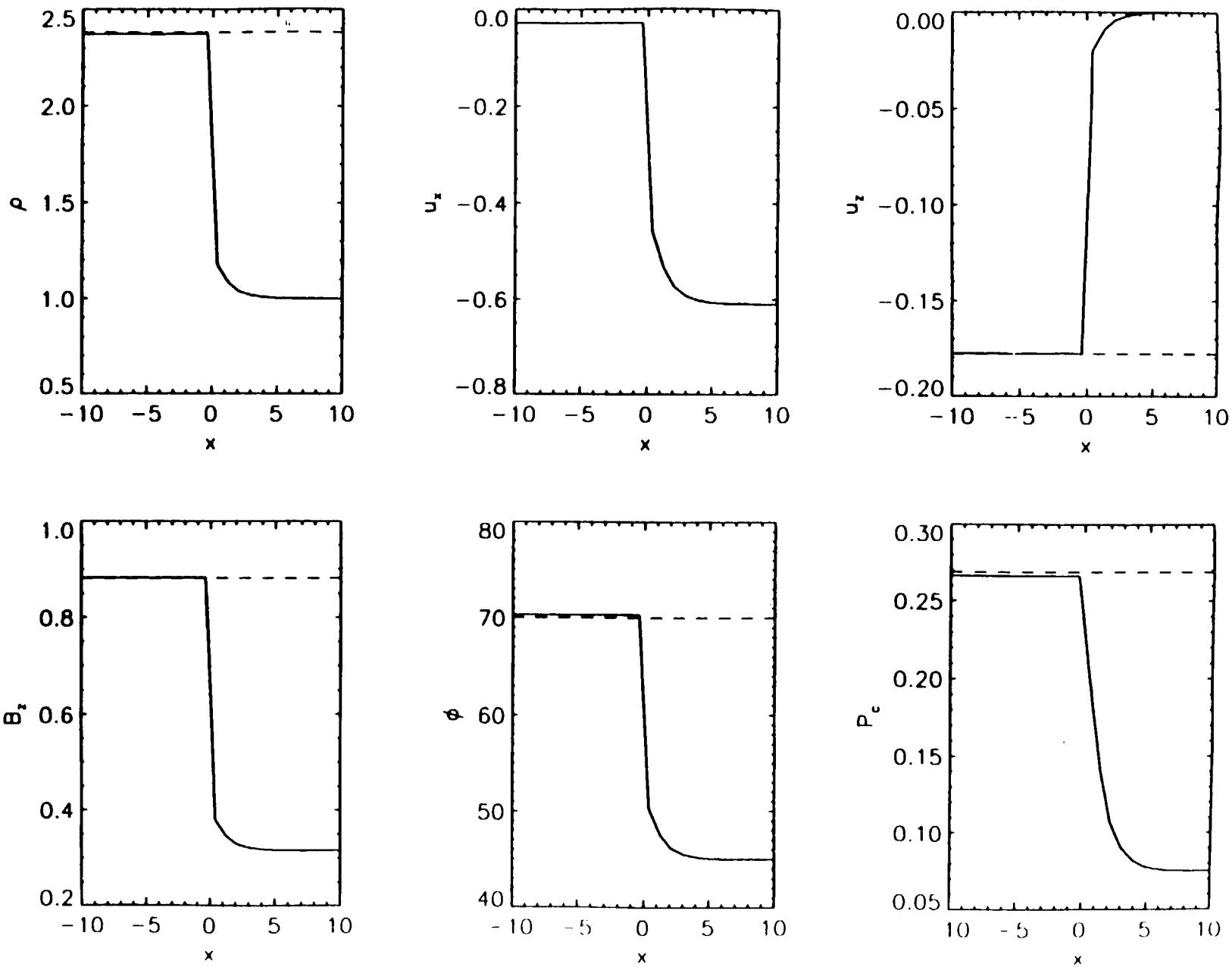
ρ
2.5
2.0
1.5
1.0
0.5
−10 −5 0 5 10
x
u_x
0.0
−0.2
−0.4
−0.6
−0.8
−10 −5 0 5 10
x
u_z
0.00
−0.05
−0.10
−0.15
−0.20
−10 −5 0 5 10
x
B_z
1.0
0.8
0.6
0.4
0.2
−10 −5 0 5 10
x
φ
80
70
60
50
40
−10 −5 0 5 10
x
P_e
0.30
0.25
0.20
0.15
0.10
0.05
10 −5 0 5 10
x

Fig. 7

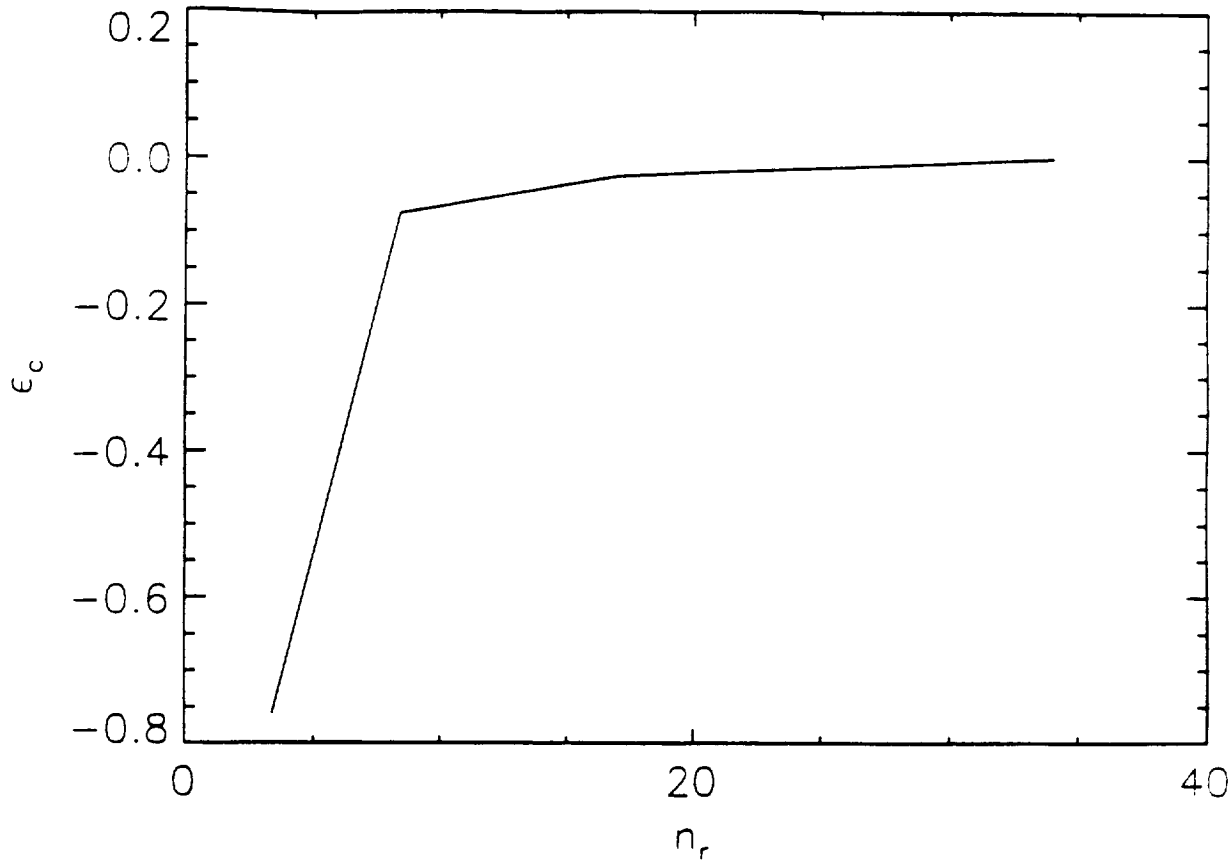

Fig. 3

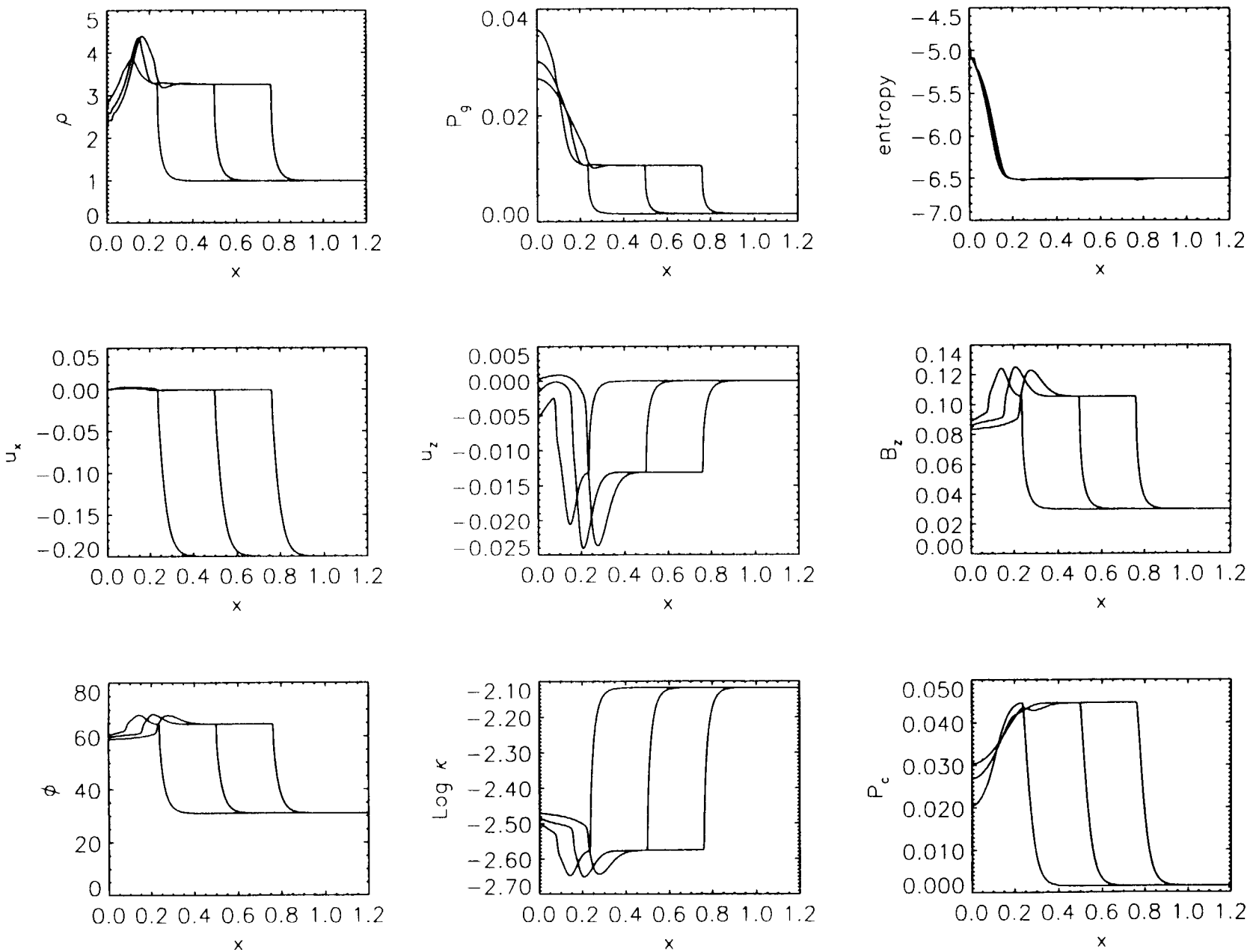

Fig 4